Proton-Proton Scattering at 40 Mev*

L. H. JOHNSTON AND D. A. SWENSON†
University of Minnesota, Minneapolis, Minnesota
(Received February 6, 1958)

Differential cross sections have been measured for the scattering of 39.4-Mev protons by hydrogen gas at angles from 45° to 4° in the laboratory system, with $\pm\frac{1}{2}°$ angular resolution at small angles. Data are given for every half degree near the interference minimum. The relative and absolute probable errors given are respectively ±0.5% and ±0.8% from 45° to 8°. The corresponding probable errors at 4° are ±4.0% and ±4.1%. The cross-section curve is essentially flat at 11.15 millibarns from 90° to 55° in the center-of-mass system. It falls to a minimum of 9.80 millibarns at 21°, and rises rapidly to 104 millibarns at 8°. A typical but not unique set of phase shifts which fit the data is: $^1S_0$, 40°; $^3P_0$, 16.90°; $^3P_1$, −6.93°; $^3P_2$, 3.04°; $^1D_2$, 2.16°; coupling parameter between $^3P_2$ and $^3F_2$ as defined by Stapp, −2.21°.

I. INTRODUCTION

A SYSTEMATIC investigation of the nucleon-nucleon interaction at energies from zero up to roughly 100 Mev is now pertinent for two foreseeable objectives. It provides particularly useful data to guide the continuing search for a satisfactory theory of this fundamental interaction, since at these energies a completely relativistic theory is not imperative.[1] Secondly, since the internal energies of nucleons in nuclei fall in this energy region, this empirical knowledge of the nucleon-nucleon interaction supplies basic information for promising theories of complex nuclei based on two-body forces, such as that of Brueckner.[2]

From the standpoint of determining phase shifts to describe proton-proton scattering, it is very desirable that angular distributions be taken to include accurate cross sections in the region of small scattering angles, where small nuclear phase shifts may be seen by their interference with the strong Coulomb phase shifts. This is a difficult region, experimentally. It is very helpful to the disentanglement of the phase shifts at higher energies if the phase shifts can be followed as a function of energy, beginning at the lowest energy at which P waves should begin to appear in definitely measurable amounts.[3]

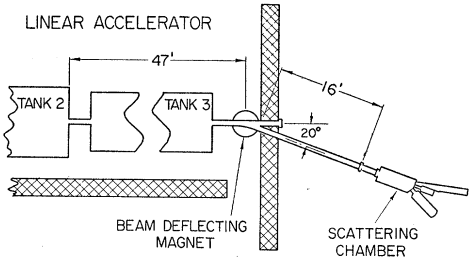

FIG. 1. General experimental layout, showing the end of tank 2, a foreshortened view of tank 3, and the relative position of the scattering chamber. Concrete shielding walls are shown as cross-hatched areas.

Experiments to date have covered quite completely the energies below 8 Mev, where Van de Graaff generators and cyclotrons have long been available; and the recent work at Harvard[4,5] at 95 Mev has begun the exploration of the higher energies of this region. In between these energies, data have been obtained[6–12] at a relatively few isolated energies as a new machine, or a new adjustment of an older one, made protons of a new energy available. Many of these experiments are of the nature of preliminary explorations, which need to be followed up by experiments which are more accurate, or which cover an extended angular range to include the Coulomb interference region.

The present work at 40 Mev was performed with the Minnesota linear accelerator, which has made available protons at 68, 40, and 10 Mev, and at certain intermediate energies. The major emphasis has been placed on obtaining reliable cross sections at angles substantially smaller than that of the interference minimum, which in this experiment occurs at 10° in the laboratory system.

II. EXPERIMENTAL APPARATUS

A. General Layout

The experimental layout is shown in Fig. 1. The Minnesota Linear Accelerator consists of a 0.5-Mev injector and three rf accelerating tanks. Proton beams are available at 10, 40, and 68 Mev from the first, second, and third accelerating tanks. For this experiment 40-Mev protons from the second tank of the

* Supported in part by the U. S. Atomic Energy Commission.
† Now at Midwestern Universities Research Association, Madison, Wisconsin.
[1] R. Serber (private communication).
[2] Brueckner, Eden, and Francis, Phys. Rev. **98**, 1445 (1955).
[3] G. Breit (private communication).
[4] Birge, Kruse, and Ramsey, Phys. Rev. **83**, 274 (1951).
[5] Kruse, Teem, and Ramsey, Phys. Rev. **101**, 1079 (1956).
[6] Allred, Armstrong, Bondelid, and Rosen, Phys. Rev. **88**, 433 (1952). (9.7 Mev).
[7] B. Cork and W. Hartsough, Phys. Rev. **94**, 1300 (1954). (9.7 Mev).
[8] F. E. Faris and B. T. Wright, Phys. Rev. **79**, 577 (1950). (12.4 Mev).
[9] Wilson, Lofgren, Richardson, Wright, and Shankland, Phys. Rev. **72**, 1131 (1947). (14.5 Mev).
[10] J. L. Yntema and M. G. White, Phys. Rev. **95**, 1226 (1954). (18 Mev).
[11] W. K. H. Panofsky and F. L. Fillmore, Phys. Rev. **79**, 57 (1950). (30 Mev).
[12] Cork, Johnston, and Richman, Phys. Rev. **79**, 71 (1950). (32 Mev).

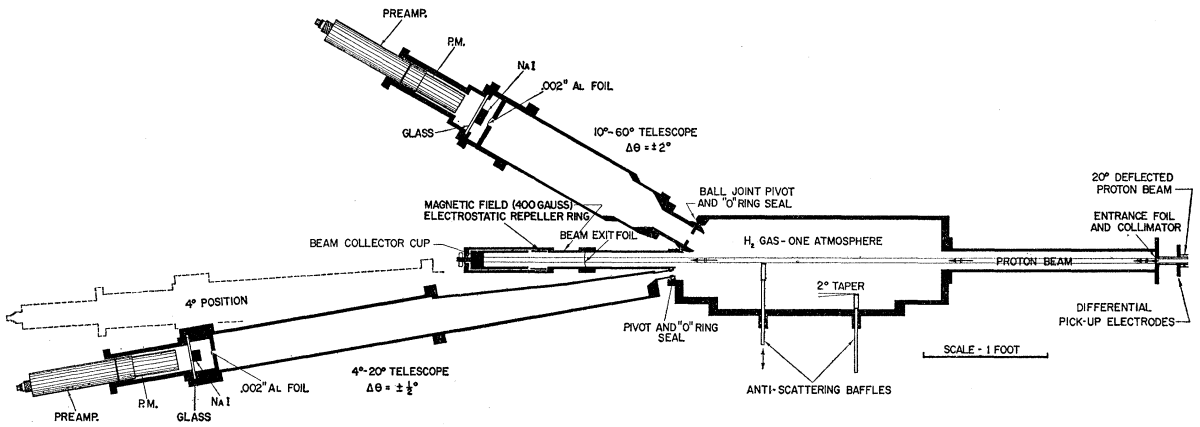

FIG. 2. Plan view of the scattering chamber showing a relatively small scattering chamber body and two large external detector telescopes. The telescopes are used independently to cover different portions of the desired angular range.

accelerator were allowed to drift[13] through the third tank. On emerging from the third tank the proton beam is bent through an angle of 20° and collimated by a three-eighths inch diameter brass collimator. The protons then travel sixteen feet to the input collimator and the entrance foil of the scattering chamber.

B. Scattering Chamber

The scattering chamber was designed to satisfy two major considerations. The first is the need to extend the differential cross sections to small angles, well below the Coulomb-nuclear interference minimum. Another consideration is the desire to obtain an absolute accuracy of 1% or better for the experimental data. A plan view of the scattering chamber is shown in Fig. 2.

The scattering chamber consists of two large external detector telescopes attached to a relatively small body of the scattering chamber, by means of vacuum-tight ball joints. These ball joints allow the telescopes to be rotated to various scattering angles without disturbing the high purity of the scattering gas. Wide detector apertures (slits) and consequently long detector telescopes are used to reduce the error introduced into the experimental data by the slit-penetrating properties of the protons. Two detector telescopes are employed in order to obtain data over the angular range of interest. One telescope covers the angular range from 4° to 20° (laboratory) with an angular resolution of $\pm\frac{1}{2}°$. High angular resolution is needed where the Coulomb part of the cross-section curve changes rapidly with angle. The second telescope covers the angular range from 10° to 60° with an angular resolution of $\pm 2°$. In this range the laboratory cross section continues to decrease slowly with angle, and one needs the additional counting efficiency afforded by shortening the detector telescope and widening its slits.

The beam enters the chamber by passing through the entrance collimator and entrance foil. The entrance collimator is a circular aperture of one centimeter diameter. The 0.0005-inch Mylar entrance foil separates the scattering gas from the accelerator vacuum. This beam of protons travels a distance of 140 cm in the scattering gas before passing through the beam exit foil. The total beam passing through the chamber is measured by collecting the unscattered protons in a beam collector cup connected to a beam current integrator. The beam exit foil (0.002-inch aluminum) separates the scattering gas from the vacuum surrounding the beam collector cup.

The scattering chamber is equipped with a set of ten antiscattering baffles, only two of which are shown in Fig. 2. Eight are located on the same side of the chamber as the 4°–20° telescope and two are located on the same side as the 10°–60° telescope. A chosen one of these baffles, the choice being determined by the angle of observation, cuts off much of the unwanted proton flux illuminating the front telescope slit. The remaining baffles are removed far from the beam by means of their vacuum-sealed shafts. Protons scattered from the front edge of the baffle cannot strike the front telescope slit due to the 2° taper on the edge of the baffle.

C. Detectors

Scattered protons selected by the detector telescope are detected by means of a single thick NaI(Tl) scintillating crystal. The NaI crystal is contained in an evacuated detector capsule which is detachable from the telescope. NaI was chosen in preference over other scintillating materials because of its low sensitivity to neutrons. For the same reason care was taken in the construction of the crystal capsule to avoid the use of any organic materials, which might provide knock-on protons in a neutron flux. The protons enter the capsule by passing through a 0.002-inch aluminum foil. The crystal is prepared by polishing the front and rear facets and sanding the four side facets. Light passes out of the crystal capsule through a one-quarter inch thick

[13] No rf accelerating field in the third tank.

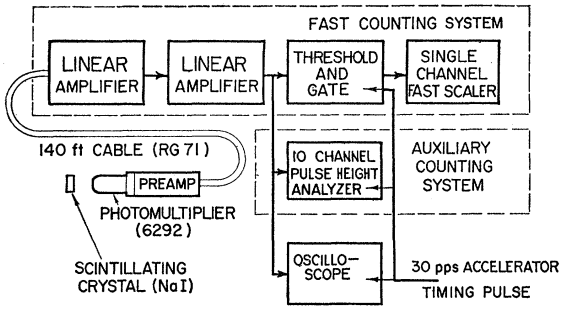

FIG. 3. Block diagram of the counting electronics.

window of glass, through approximately 2 inches of air, and into a photomultiplier tube (Dumont 6292).

D. Counting Electronics

A block diagram of the counting electronics is shown in Fig. 3. Electrical pulses from the photomultiplier pass directly into a cathode follower circuit. The input circuit of the cathode follower is designed to give a pulse which rises to a maximum in one-quarter microsecond and decays to zero in a half microsecond. The pulses from the low impedance output of the cathode follower are transmitted a distance of 140 feet to the counting room by means of a doubly shielded 93-ohm coaxial cable (RG-71).

The pulses arriving in the counting room are amplified by a pair of linear amplifiers each with a gain of 8. The pulses are then fed into a threshold and gating circuit, such that pulses pass through the circuit only if they arrive during the "on" time of the accelerator.[14] The pulses are then counted by a Hewlett-Packard High Speed Decade Scaler Model 520A, having a recovery time of 0.1 microsecond. The number of counts obtained from this scaler is the number used in the calculation of cross sections. This branch of the proton detection system is referred to as the fast counting system.

The same amplified pulse that is fed into the threshold and gating circuit of the fast counting system is fed into an auxiliary 10-channel pulse-height analyzer,[15] having a recovery time of 5 microseconds. This auxiliary pulse-detection system makes it possible to monitor the entire pulse-height spectrum, and hence provides a means of setting the threshold of the fast counting system to include the entire elastic pulse-height peak. From such a pulse-height spectrum, one also obtains the energy resolution of the detection system, the relative amounts of elastically scattered protons to background counts, and the energy distribution of the background counts.

[14] The "on" time of the machine for this experiment consisted of a 200-microsecond pulse, repeated 30 times per second.

[15] C. W. Johnstone, Nucleonics **11**, No. 1, 37 (1953).

III. TARGET GAS

The target material in this experiment was hydrogen gas at a pressure slightly above one atmosphere. Tank hydrogen was purified by passing it through a palladium filter, which has been described[12] previously. Evolution of contaminating gases by the walls of the scattering chamber was found to give a rate of pressure rise of 3×10^{-4} mm of Hg per minute, on an ionization gauge. As a test of the nature of this gas, the evacuated chamber was sealed off for a period of three hours, and the scattering measured from the accumulated gases, whose pressure then read 60 microns on a thermocouple gauge. The cross section measured at 4° laboratory was consistent with Rutherford scattering from oxygen. From these tests it was decided to change the gas at least every 12 hours, and oftener if working at less than 20°. The palladium tube was tested for perforation after each filling, by a helium leak tester.

A mercury manometer was used to measure the gas pressure. It was connected to the chamber only while readings were being taken, to avoid contamination. The chamber temperature was read by a thermometer embedded in the metal near the scattering region. Temperature and pressure readings were taken every two or three hours of operation. Sometimes the Mylar beam entrance window leaked enough to reduce the hydrogen density at the rate of 0.1% per hour. In calculating the density of scattering nuclei, correction was made for mercury temperature, acceleration of gravity, and Van der Waals forces.

IV. GEOMETRY CALCULATIONS

Since in this geometry the 4° scattering volume becomes quite long, new calculations were made of the geometrical formulas.[16,17] We assume the incident beam to be a uniform circular cylinder having no divergence, and radius b. Both telescope slits are assumed rectangular, the first being of infinite height perpendicular to the plane of Fig. 4, and the detector slit being of height $2h$. Other geometrical parameters are defined in Fig. 4. If C is the number of detector counts, B the number of incident protons, N_0 the number of scattering

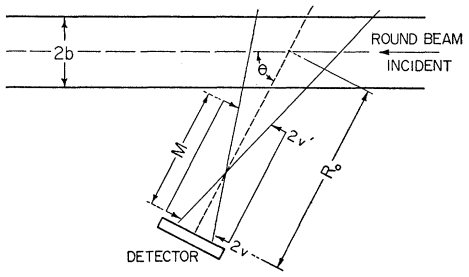

FIG. 4. Basic counting geometry.

[16] Allred, Rose, Tallmadge, and Williams, Rev. Sci. Inst. **22**, 191 (1951).

[17] C. L. Critchfield and D. C. Dodder, Phys. Rev. **75**, 419 (1949).

nuclei per cubic centimeter, and $d\sigma/d\Omega$ is the laboratory cross section, our result[18] to second order in the dimensions is

$$C=BN_0\frac{d\sigma}{d\Omega}\frac{2v'2v2h}{MR_0\sin\theta}\left[1+\frac{v^2\cot^2\theta}{3R_0^2}-\frac{v'^2+v^2}{2M^2}+\frac{b^2}{4R_0^2\sin^2\theta}-\frac{3b^2}{8R_0^2}-\frac{h^2}{2R_0^2}\right].$$

The significance of the terms in the brackets is as follows: the term $v^2\cot^2\theta/3R_0^2$ corrects for horizontal asymmetry of the scattering length, upstream and downstream from center along the incident beam. Two-thirds of the term $(v'^2+v^2)/2M^2$ corrects for horizontal obliquity of the protons at the first telescope slit, and one-third of it is for horizontal obliquity at the detector slit. The term $b^2/(4R_0^2\sin^2\theta)$ corrects for horizontal width of the beam, which varies the radius for scattering element to detector element. The term $3b^2/8R_0^2$ is for vertical obliquity at the detector slit due to height of the incident beam; and $h^2/2R_0^2$ is for vertical obliquity at the detector slit due to height of the detector slit. The sum of these corrections amounts to less than 0.2% at all angles for each telescope.

Table I gives approximate numerical values for the geometrical parameters defined above. The parameter R_0 is a simple function of the angle θ and the perpendicular distance A from the telescope pivot axis to the axis of the cylindrical proton beam.

V. EXPERIMENTAL PROCEDURE

A. Alignment of the Scattering Chamber

Because of the desire to obtain accurate data at small angles, the alignment of the scattering chamber and the telescopes relative to the incident beam is very critical. For example, at 4°, an error of 0.01° in the measured angle causes a 1% error in the measured cross section.

TABLE I. Approximate geometrical dimensions of scattering chamber. All parameters are defined graphically in Fig. 4, with the exception of A which is the perpendicular distance from the telescope pivot axis to the axis of the cylindrical proton beam.

Parameter	4°–20° telescope	10°–60° telescope
$2b$	1.0 cm	1.0 cm
M	114 cm	57 cm
$2v$	1.1 cm	2.0 cm
$2v'$	1.1 cm	2.0 cm
$2h$	2.8 cm	8.0 cm
A	3.4 cm	5.8 cm

The scattering chamber is rigidly fastened to a three-legged frame. Each leg rests on a set of positioning screws, which provide vertical and lateral adjustment. The 20° deflected beam was located in space by allowing it to form a darkened image on a glass plate. The chamber was then roughly aligned with this beam and the one-centimeter diameter entrance collimator was centered on the beam. The entrance foil was removed and the chamber was evacuated to provide a sharp image of the entrance collimator on a glass plate at the exit end of the chamber. The axis of the scattering chamber was aligned with the center of the darkened image, care being taken not to move the entrance collimator. It is believed that this alignment was done to about ±0.01 inch.

The axes of the 4°–20° telescope and the cylindrical beam were defined by taut wires, and the angle between them was adjusted by triangulation to 4°. The pointer mounted on the telescope was adjusted to the 4° mark on the ruled angular scale rigidly fastened to the scattering chamber body. The 10°–60° telescope was geometrically aligned in a similar manner. Angular settings of the telescopes using the pointer and scale are reproducible to 1/50°. To improve the reproducibility of the 4° angle, a mechanical stop was placed on the scale at this point.

As a later check on the angle calibration, the same apparatus was used to measure the cross section of argon gas for 10-Mev protons at an angle of 4°. Optical model calculations at this energy and angle predict[19] a cross section about 1% greater than Rutherford scattering. Our argon result is 5% greater than the Rutherford cross section, which could be interpreted to indicate that the angular scale was reading angles 0.04° larger than true angle. However there is sufficient doubt about the optical model predictions at these angles that we prefer to regard this as a rough check of the angular setting, and to assign correspondingly large probable errors to the angle calibration.

B. Measurement of Beam Charge

The space for the beam collector was rather restricted in this experiment by the requirement of locating the detector telescope close to the beam when scattering at 4°. This called for the compact geometry shown in Fig. 5. The beam is stopped in lead in the bottom of the collector cup, which is quite deep to discourage escape of secondary electrons. The "repeller ring" is intended to repel secondary electrons from both the foil and the cup; and the 400-gauss magnetic field is to deflect the highest energy electrons produced in the foil. In practice neither was found to be necessary, as shown in tests where the magnetic field was removed, and the

[18] It is instructive to compare this with the results of Critchfield. When his formula as quoted in reference 16 is specialized to $\alpha=90°$, $m=0$, it agrees with the first three terms of the six terms in our bracket; it omits the last three because it does not attempt to take into account finite beam diameter and detector height. When the geometrical formula in reference 17 is adjusted for non-diverging beam (set his $L=S_0=\infty$) and rectangular detector aperture (instead of round), it is consistent with all of our terms. For a circular detector window he would change the coefficient $\frac{1}{2}$ in our sixth term to $\frac{3}{8}$.

[19] Glassgold, Cheston, Stein, Schuldt, and Erickson, Phys. Rev. **106**, 1207 (1957).

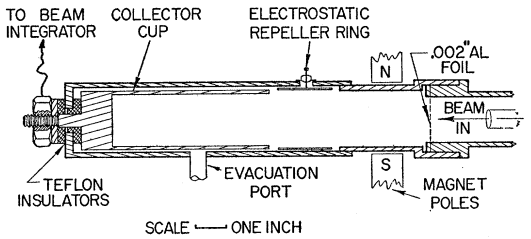

FIG. 5. Beam collector. The beam is stopped in a lead slug deep within a brass collector cup. Provisions are made for application of electric and magnetic fields for the purpose of controlling secondary electrons.

repelling voltage was varied between zero and -5000 volts, with no significant effect on the measured cross section when counting 20 000 protons. All final data were taken with the magnetic field present and the repeller ring grounded. A vacuum of about 5×10^{-5} mm of Hg was maintained in the cup during runs.

The beam current integrator system uses a standard 100% feedback circuit with electrometer tube input and a gain of 10 000. The collector cup thus only changes potential by 10 millivolts while the integrating capacitor is charged to 100 volts. Three different integrating capacitors were used in this experiment, selectable by a rotating switch to correspond to the magnitude of beam being used. The capacitor voltage (about 100 volts) was divided 100:1 by a 10 000-ohm precision resistance divider and read at the one-volt level by an L and N potentiometer.

Two methods were used for determining the charge calibration of the integrator. The first involved measurement of the capacitance and the charging voltage. The capacitors were compared to a type 722-D General Radio Variable Air Capacitor by means of an impulse bridge. The measurement was made with the integrating capacitors in their normal environment and connected in their normal relationship to "ground," to avoid changing stray capacitances.

The second method was to measure the over-all charge calibration directly by injecting a known charge at the normal, slow rate into the integrator. The source of standard charge is shown in Fig. 6. It consists of a standardized 3-terminal shielded 0.001-μf air capacitor C_1 which has a leakage time constant exceeding 3000 hours, and a potentiometer P_1 to charge one end of it to a precisely known potential. The speed of charge delivery is proportional to the speed of manual rotation of P_1. The left-hand end of C_1 remains essentially at ground potential due to the feedback properties of the integrator circuit. The charge calibration of the integrator was found to be about 0.2% higher when the calibrating charge was delivered slowly over a period of $\frac{1}{2}$ hour, than when it was charged in $\frac{1}{10}$ second. This is taken to be due to soakage in the polystyrene capacitors, since separate allowance is made for grid current in the electrometer tube. The capacitor C_1 was standardized with an impulse bridge against a General Radio type 1401-D Fixed Air Capacitor, and against a General Radio type 722-D Variable Air Capacitor, both being advertised as good to 0.1%.

C. Control and Measurement of Beam Energy

The mean energy of the linear accelerator is a function of the tuning conditions of the machine. Variations of the mean energy of as much as plus or minus $\frac{1}{2}$% have been noticed under extreme tuning conditions. To eliminate such fluctuations in energy, the operator was supplied with an energy monitor to enable him to keep the energy constant. This indication of beam energy was provided by a pair of differential pickup electrodes which sense the position of the 20° deflected beam. A small portion of the beam strikes the two electrodes, with a major portion of it passing between them into the scattering chamber. If the magnetic field is held constant, the position of the beam spot is a unique function of the energy of the machine. The operator then tunes the machine so that an equal amount of beam hits each of the pickup electrodes as indicated remotely in the control room.

A relative indication of the magnetic field in the gap of the deflecting magnet, accurate to 0.1%, is provided by a current balance. This consists essentially of a d'Arsonval galvanometer movement placed in the magnetic field of the deflecting magnet. A balance is indicated when a precisely measured current through the galvanometer coil produces enough torque (about 300 g-cm) to begin lifting a lead counterweight. The purpose of the current balance is to enable one to reproduce a specific magnetic field, and hence a specific beam energy, to a high degree of accuracy over periods of many years if necessary.

A spectrometer for analyzing the spectrum of energies present in the proton beam was constructed using the 20° deflecting magnet, shown in Fig. 1, as the analyzing magnetic field. Collimation for the spectrometer was provided by a pair of slits (slits A and B in Fig. 7) 0.020 inch wide, separated by 40 feet. The beam was deflected approximately 20° and was analyzed by use of a 0.020-inch slit (slit C in Fig. 7) at a distance of 16 feet from the magnet. The spectrum was investigated by sweeping it across the fixed slit by changing the magnetic field. The extremely small beam current passing through the analyzing slit was measured by means of an air ionization chamber. A relative indication of the magnetic field was provided by the current balance.

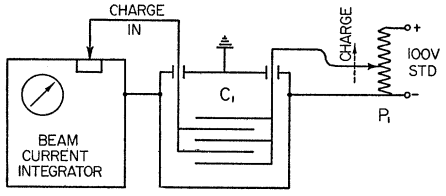

FIG. 6. Circuit used for calibration of beam current integrator.

The energy calibration of the magnetic spectrometer was accomplished by the floating-wire technique,[20] the essential features of which are shown in Fig. 7. A close analogy exists between the trajectory of a beam of charged particles of momentum mv and charge q in a magnetic field, and the trajectory of a flexible wire carrying a current I and subjected to a tension T in the same field. If one adjusts the trajectories to be identical, the relation $mv/q=T/I$ holds.

A "cold" wire (no current) was strung from the center of slit B to point D, which had experimentally been found to line up with slits A and B. By sighting vertically on the two wires at point E and adjusting the current in the floating wire, the horizontal coordinates of the floating wire could be made to coincide with the horizontal coordinates of the proton beam before deflection. The horizontal coordinates of the floating wire and the proton beam coincided at the spectrometer analyzing slit C; hence the horizontal projection of the floating wire was identical to that of the proton beam. The momentum and hence the energy of the corresponding proton beam were computed.

The effect of the gravitational force is to cause the wire to sag. The vertical coordinate of the wire is insignificant except in the region between the magnet pole pieces. The ends of the floating wire were raised about $\frac{1}{8}$ inch at slit B and $\frac{1}{2}$ inch at slit C in order that the trajectory of the floating wire would be horizontal and centered vertically in the magnet gap. The tension of the wire in the gap was taken as the horizontal component of the tension at slit C.

Typical values for the current and tension applied to the 0.006-inch diameter copper wire were 1 ampere and 100 grams-force. The wire was annealed in its trajectory by increasing the current to 3 amperes and providing enough tension to hold the wire in position.

Hence the energy spectrum obtained by plotting the relative beam intensity as a function of current balance reading can be calibrated in terms of the corresponding proton energy for any value of current balance reading. Figure 8 shows three such sets of data, and three points at which the energy spectrum was calibrated in terms of energy. The mean accelerator energy is 39.70 Mev, and the spread in energy is about $\pm\frac{1}{2}\%$. The beam is degraded to an energy of 39.40 Mev before scattering.

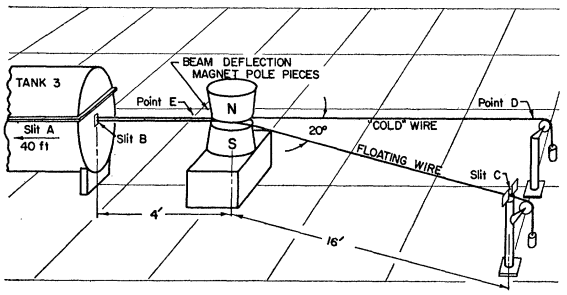

FIG. 7. Experimental layout for the floating-wire energy calibration. Magnet yoke and vacuum pipes are not shown.

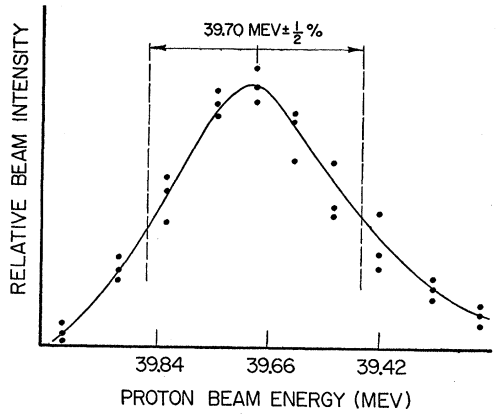

FIG. 8. Energy spectrum of proton beam. Three points at which the energy spectrum was calibrated are shown on the abscissa. Although the mean energy is taken to be 39.70 Mev, the protons at the scattering region have been degraded to 39.40 Mev.

D. Final Procedure

Before filling the scattering chamber with hydrogen gas, the chamber was evacuated for a period of at least 12 hours to a pressure of 4×10^{-5} mm of Hg or less, and a rate of rise of less than 2×10^{-2} mm of Hg per hour. The inner volume of the palladium tube hydrogen purifier and its connecting pipes were evacuated. The region surrounding the palladium tube was alternately evacuated and flushed several times with commercial tank hydrogen (99.5% pure) before being filled to a pressure of 100 psi. When the palladium tube was heated, the purified hydrogen passed into the scattering chamber filling it to a pressure of one atmosphere. During the experimental run the chamber was isolated by valves from the hydrogen purifier, the oil diffusion pump, the liquid air trap, and the mercury manometer. The pressure was measured periodically between experimental runs for as long as the filling of hydrogen was used (up to twelve hours in certain cases).

The detector telescope was set at the desired angle and the corresponding antiscattering baffle was placed in its correct position. With the aid of the current balance, the magnet current regulator was periodically adjusted during each run to give the desired magnetic field in the 20° beam deflecting magnet.

The threshold of the fast counting system was adjusted such that this system counts all pulses falling in channels 5 and above of the 10-channel pulse-height analyzer. Since the operation of pulse-height discriminator circuits is sensitive to the pulse shape, a comparison of thresholds can best be done with a pulse identical in shape to the pulses to be counted. The photomultiplier gain was set so that many proton pulses fell in channels 4 and 5, and short runs of 50 counts were made. The threshold of the fast counting

[20] L. Cranberg, Los Alamos Scientific Laboratory, Atomic Energy Commission Report AECU-1670, 1951 (unpublished).

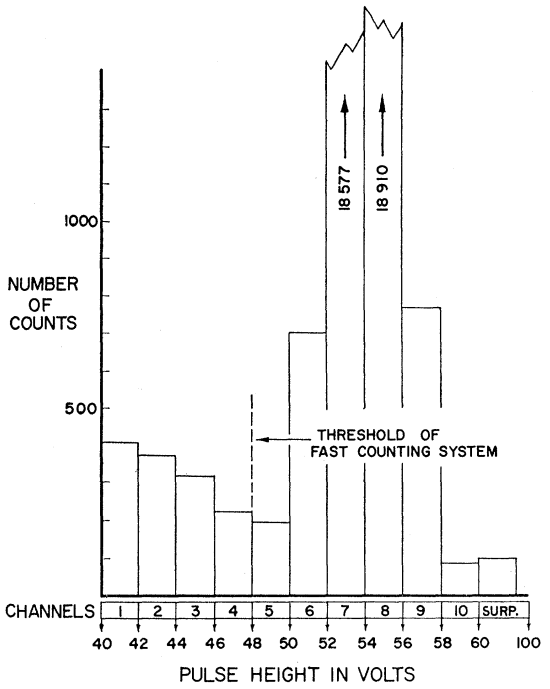

FIG. 9. Typical pulse-height distribution. The fast counting system counts all pulses falling to the right of the fast counting system threshold.

system was adjusted so that the number of counts in the fast system was equal to the sum of the counts in channels 5 and above.

The photomultiplier gain was then adjusted so that the elastic proton peak fell entirely within channels 5 and above of the 10-channel pulse-height analyzer. A typical pulse-height distribution is shown in Fig. 9. The above procedure enables the fast counting system to count all pulses in the pulse-height peak, without counting a significant amount of slit-scattered protons or background counts.

The beam current through the chamber was adjusted to give an average counting rate of 10 counts per second, and a probable counting loss for the fast system of 0.1% (one second contains approximately 6000 microseconds of accelerator "on" time). The beam integrating capacitor was discharged and the zero of the beam current integrator was checked with a potentiometer. The beam was then turned on to start a typical run of 40 000 counts. The run was interrupted when and if the feedback voltage of the beam current integrator reached 100 volts, in which case the voltage was read with a potentiometer (to better than 0.1%), the capacitor discharged, and the run resumed.

Neutrons and γ rays originating from the entrance collimator and the beam collector cup are the chief constituents of the background. The effect of this background was reduced by placing lead shielding around the entrance collimator, and placing as much lead between the beam collector cup and the detector crystal as the telescope would allow. The intensity of background counts was insignificant over most of the angular range. Only for angles greater than 38° was it necessary to take background runs. The typical background correction in percentage of total counts for data taken at 40° is 0.15%, and at 45° is 0.35%.

VI. CORRECTIONS

A. Evaluation of Slit-Scattering Corrections

The detector telescopes were designed to have sufficiently large-scale geometry that the slit-scattering corrections would be 1% or less (slit width of 4°–20° telescope, 1 cm; slit width of 10°–60° telescope, 2 cm). It was desired that this correction be known to such a degree that the residual error would be 0.1% or less. Such corrections can be calculated theoretically under ideal circumstances.[21] However, these circumstances are far from being met, especially for the front slit of the telescope. It was found possible to evaluate the correction experimentally. Two experiments were conducted; one enabling the slit-scattering correction for the front slit to be measured, and the other providing similar information for the rear slit.

In the case of the first experiment, a plug was placed in the front slit, making in effect two narrow slits (0.008 inch wide) precisely in the position of the edges of the ordinary slit. The plug side of these narrow slits was tapered ($\frac{1}{2}$° in the case of the 4°–20° telescope) to allow full view of the detector from the slit surfaces. The plug doubles the amount of slit scattering and reduces the proton-proton scattering by a factor of 50, thus greatly enhancing the relative effect of the slit scattering. This experiment was conducted with the correct antiscattering baffle in position.

The second experiment involved measuring the counting yield of a telescope as a function of the width of a variable slit installed towards the rear of the 10°–60° telescope. The counting yield is a linear function of the rear slit width as long as care is taken not to make the slits so narrow as to alter either the illumination of the slits or the detection of protons from the slits. The

TABLE II. Slit-scattering corrections, as determined experimentally. This correction factor when applied to the data reduces the number of counts.

Telescope	Lab angle	Front slit apparent additional slit width (inches)	Rear slit apparent additional slit width (inches)	Total correction factor
4°–20°	4°–10°	0.0007	0.0022	0.9925
	11°–20°	0.0007	0.0020	0.9929
10°–60°	10°–19°	0.0015	0.0020	0.9955
	20°–29°	0.0017	0.0016	0.9957
	30°–39°	0.0020	0.0012	0.9959
	40°–49°	0.0024	0.0007	0.9961
	50°–59°	0.0026	0.0003	0.9963

[21] E. Courant, Rev. Sci. Instr. 22, 1003 (1951).

intercept for zero slit width represents the counting yield due to scattered protons.

The slit-scattering corrections are presented in Table II, both as the apparent additional slit width for each slit of the two telescopes, and as the total correction factor by which the measured cross section was multiplied to give the cross sections corrected for slit scattering.

B. Correction for Inelastic Nuclear Reactions

When a thick scintillation detector is used to count protons of energy greater than 10 Mev, an appreciable number of the protons make inelastic nuclear reactions in the scintillating material.[22] These protons make substandard pulses in the pulse-height detector system. Hence the protons entering the detectors in this experiment produce a peak of standard height pulses, along with a low-pulse-height tail. Most of this tail is chopped off by a threshold circuit incorporated into the fast-pulse detector system to discriminate against low-energy background and slit-scattered protons. Hence a correction is required to account for the substandard pulses of the low-pulse-height tail, which are discarded by the threshold circuit.

This correction was determined for the protons of 40, 28, and 10 Mev by producing a $\frac{1}{8}$-inch wide beam of protons free from low-energy components, and letting it strike the center of a $\frac{3}{4}$-inch wide NaI(Tl) crystal detector under conditions of negligible background. The pure beam was produced by first collimating to 0.1 milliradian and magnetically analyzing to reject slit-scattered protons. The pulse-height distribution yields the required correction (Table III) for various discriminator settings. A typical pulse-height distribution is shown in Fig. 10. The magnitude of the correction can be interpreted as an effective inelastic reaction cross section for protons incident on sodium and iodine nuclei, amounting to roughly $\frac{3}{4}$ of the geometrical cross section ($r_0=1.3\times10^{-13}$ cm). In order to apply these corrections to the proton counts taken at various angles (energy changes with angle) and for particular discriminator settings, the table was interpolated on the basis of the assumption that the correction varies linearly with range in sodium iodide.

TABLE III. NaI inelastic nuclear reaction correction due to the chopped-off low pulse-height tail from the scintillator. This correction is expressed as a percentage of total number of counts in the pulse-height peak and, when applied, increases the number of counts.

Energy Mev	Threshold setting (in percentage of peak pulse height) 50%	60%	70%	80%	90%
40	1.14	1.45	1.68	1.95	2.10
28	0.73	0.89	1.00	1.10	1.14
10	0.22	0.27	0.31	0.34	0.37

[22] This was first called to our attention by Robert Eisberg.

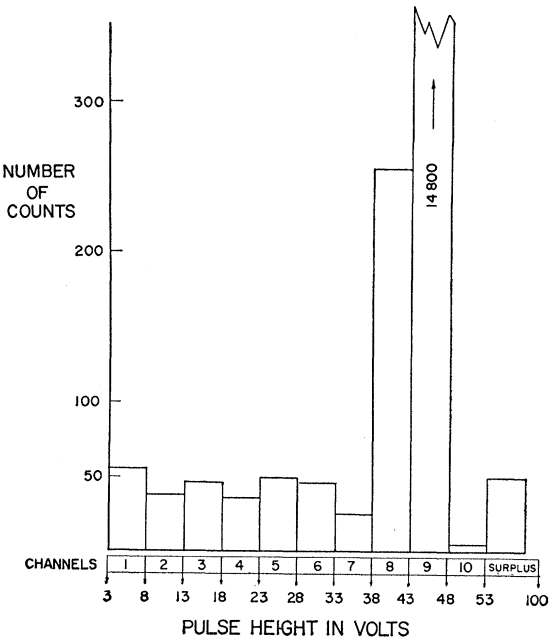

FIG. 10. Typical pulse-height distribution obtained during evaluation of the correction for inelastic nuclear reactions in NaI(Tl).

C. Corrections for Finite Angular Resolution

There exists some differential cross section $\sigma(\theta)$ which one is interested in measuring by using a sensing device with a finite angular resolution $R(\theta)$. The resolution function expresses the fact that although one is attempting to determine the differential cross section $\sigma(\bar{\theta})$ at $\bar{\theta}$, the sensing device is also partially sensitive to the protons scattered within the range $\bar{\theta}\pm\Delta\theta$.

Consider the identity

$$\sigma(\bar{\theta})=\int R(\theta)\sigma(\theta)d\theta\Big/\int R(\theta)d\theta$$

$$+\int R(\theta)[\sigma(\bar{\theta})-\sigma(\theta)]d\theta\Big/\int R(\theta)d\theta,$$

where the integration is over the nonzero portion of the resolution function. The term on the left-hand side is the true cross section at $\bar{\theta}$. The first term on the right-hand side is precisely the cross section [to be denoted by $\sigma_m(\theta)$] measured by using a telescope with resolution function $R(\theta)$. The second term on the right-hand side cannot be evaluated because of an ignorance of the function $\sigma(\theta)$ or the value $\sigma(\bar{\theta})$. However, if one can determine a known function $\sigma_K(\theta)$ which, except for proportionality constant C, is a good representation of the true function $\sigma(\theta)$ over the angular range $\bar{\theta}\pm\Delta\theta$, then $C\sigma_K(\bar{\theta})-C\sigma_K(\theta)$ is approximately equal to $\sigma(\bar{\theta})-\sigma(\theta)$. Using this relationship, the equation for $\sigma(\bar{\theta})$

TABLE IV. Finite angular resolution correction, which reduces the experimentally measured cross section by the given factor.

Lab angle	Correction factor
4°	0.961
5°	0.976
6°	0.988
7°	0.993
8°	0.998
8½°–45°	1.000

reduces to

$$\sigma(\bar{\theta})=\sigma_m(\bar{\theta})\left[\sigma_K(\bar{\theta})\int R(\theta)d\theta\Big/\int R(\theta)\sigma_K(\theta)d\theta\right].$$

This correction factor was calculated for this experiment at the angles 4° to 8°. The factor is not significantly different from unity at other angles. The known function $\sigma_K(\theta)$ was chosen as the laboratory cross section corresponding to one of the best fits to the preliminary data[23] obtained through a phase shift analysis.[24] The resolution function for the small-angle telescope is approximately proportional to $[\Delta\theta-|\theta-\bar{\theta}|]/\sin\theta$ for $|\theta-\bar{\theta}|\leq\Delta\theta$, where $\Delta\theta=\frac{1}{2}°$. The calculation of the bracketed correction factor was accomplished by a numerical integration. The results are given in Table IV.

D. Correction for Change in Energy at Small Angles

The energy of an incident proton for a scattering event is dependent on the total path length of hydrogen traversed. It is a feature of the design of this scattering chamber that the path length from the entrance foil to the center of the effective scattering volume is a function of the angle of the detector telescope. For angles larger than 10° the change in energy as a function of angle is insignificant. For these large angles the total path length is approximately 100 cm, and the thickness in Mev of the entrance foil and the 100 cm of hydrogen is 0.30 Mev. Hence for the majority of the cross sections the laboratory energy of the incident particle was 39.40 Mev. Only for a few of the smallest angles was the energy significantly different from 39.40 Mev.

Rather than quote a separate energy for each cross section at these small angles, the cross sections were extrapolated on the basis of a $1/E^2$ dependence to the energy 39.40 Mev. Table V gives the dependence of the incident energy on angle and the energy correction factor. The cross section quoted in the results is $\sigma(E_0)=(E/E_0)^2\sigma(E)$, where $E_0=39.40$ Mev.

TABLE V. Dependence of incident energy on angle, and energy correction factor $(E/E_0)^2$. Application of the correction factor extrapolates the measured cross sections, on the basis of a $1/E^2$ dependence, to the cross sections expected at E_0. ($E_0=39.40$ Mev.)

θ_{lab}	E (Mev)	$(E/E_0)^2$
4°	39.49	1.0045
5°	39.46	1.0030
6°	39.44	1.0020
7°	39.43	1.0015
8°	39.42	1.0010
9°	39.41	1.0005
10°	39.40	1.0000
...	...	...
...	...	...
...	...	...
45°	39.40	1.0000

[23] The preliminary data were corrected for finite angular resolution effects by choosing the Coulomb cross section as the known function.

[24] H. P. Noyes and M. H. MacGregor, University of California Radiation Laboratory Report UCRL-4947 (unpublished).

E. Multiple and Plural Scattering

The effects of multiple and plural scattering[25,26] were found to be insignificant by both theoretical and experimental means. No corrections are required to account for these effects.

The effects of multiple scattering on collection of beam charge was calculated to be less than 0.1%. The size of the beam near the collector cup was determined by exposing a glass plate to the beam. The darkened spot indicated that the beam fell well within the aperture of the collector cup. The collection of beam charge was experimentally checked by comparing the charge collected for the normally collimated beam to that collected for a beam collimated to half the normal diameter and at approximately half the normal distance from the beam current collector cup. Proton-proton scattering at 45° was used as a monitor of the total beam charge. The results were the same to within the 0.3% counting statistics of the experiment.

The effect of the multiple scattering superimposed on single-scattering events was calculated to be about 0.1% at 4° (lab). The introduction of counts due to plural scattering, for the detector telescope set at 4°, was also calculated to have less than 0.1% effect. Both of these effects give rise to a fractional increase in the measured cross section.[27] The fractional increase varies as the first or higher power of the target gas pressure. Experimental proton-proton scattering runs were made at 4° (lab) and at target pressures of 0.1, 0.5, and 1.0 atmosphere. The measured cross sections show no dependence on pressure inconsistent with the probable error of the 0.3% counting statistics.

VII. ANALYSIS OF EXPERIMENTAL ERRORS

Table VI gives a summary of errors attributed to all important sources. The entries in the absolute error column are the probable errors to be attached to the measured value of the quantity in the left-hand column. The entries in the relative error column signify the probable error of the ratio of the measured value of the

[25] E. J. Williams, Proc. Roy. Soc. (London) **A169**, 531 (1938).

[26] B. Rossi and K. Greisen, Revs. Modern Phys. **13**, 240 (1941).

[27] Breit, Thaxton, and Eisenbud, Phys. Rev. **55**, 1018 (1939).

quantity, for any two experimental points. The error contribution of the angular calibration is insignificant, except for the angles below 8°, where it rapidly becomes significant. The error contribution due to the angular calibration is taken as follows: 4°, 4%; 5°, 1.6%; 6°, 0.8%; 7°, 0.4%; 8°, 0.2%; and 9° through 45°, 0.1%. The resultant absolute and relative probable errors at each angle are listed later in Table VIII.

VIII. EXPERIMENTAL RESULTS

Table VII gives the data for two typical angles. Our final results are based on 82 such scattering runs; these represent all of the runs taken after the final operating procedure was adopted, with the exception of ten runs discarded because of known errors, and four more discarded because their results differed so greatly from that of other runs that operational errors were assumed. In addition to these datum runs, there were 39 test runs and 46 runs for evaluation of corrections. The data were collected over a period of ten months. There is no evidence of a trend for early results to be either higher or lower than later results.

The beam charge in Table VII is the measured integrated charge corrected for electrometer tube drift (insignificant in most cases). The entries in the column headed "corrected number of counts" contain the majority of corrections. This number is corrected to the expected number of counts for a target gas at STP. The number is also corrected for inelastic nuclear reactions in NaI, slit scattering, change in energy at small angles, finite angular resolution effects, background counts, electronic pileup of counts, and counting losses. The cross section is transformed from the laboratory coordinate system to the center-of-mass coordinate system by the relation $[d\sigma/d\Omega(\text{lab})]d\Omega(\text{lab}) = [d\sigma/d\Omega(\text{c.m.})]d\Omega(\text{c.m.})$. The calculation of the ratio $d\Omega(\text{lab})/d\Omega(\text{c.m.})$ was done relativistically.[28] The corrected cross section is given in the last column of Table VII.

Table VIII lists the mean value of the cross section for each laboratory angle, and for center-of-mass angles. Individual runs are weighted in terms of the number of counts in each. The rms deviation from the mean is less than 1% for all angles, and with the exception of 3 angles, is less than 0.7%. The fourth and fifth columns list the absolute and relative error assigned to the given value of the cross section.

Figure 11 gives the over-all features of the experi-

TABLE VI. Summary of experimental errors.

Source of error	Absolute error	Relative error
Beam current errors		
Capacity	±0.2%	±0.1%
Voltage	±0.1%	±0.1%
Electrometer drift	±0.1%	±0.1%
Collection of stray charges	±0.2%	0
Counting errors		
NaI inelastic nuclear reaction	±0.3%	±0.1%
Slit scattering	±0.2%	±0.1%
Counting statistics	±0.3%	±0.3%
Counting losses	±0.1%	±0.1%
Geometry errors		
Geometry calculation	±0.4%	±0.1%
Angle calibration[a]	±0.1%	±0.1%
Target errors		
Target temperature	±0.1%	±0.1%
Target pressure	±0.1%	±0.1%
Gas impurities	±0.1%	±0.1%
Beam energy errors		
Mean energy	±0.3%	±0.1%
Energy dependence on angle	±0.1%	±0.1%
Total error[a]	±0.8%	±0.5%

[a] The angle calibration error is valid for all angles except 4°, 5°, 6°, and 7° (see text).

TABLE VII. Experimental results of typical proton-proton scattering runs.

Laboratory angle[a]	Beam charge (microcoulombs)	Corrected number of counts	Corrected cross section (c.m.) (mb/sterad)
13½° LA	0.1109	44 403	10.31
13½° LA	0.1109	43 910	10.20
13½° SA	3.4210	45 472	10.29
40° LA	0.2862	43 350	11.18
40° LA	0.2773	41 736	11.11
40° LA	0.2899	43 930	11.19

[a] SA indicates experimental runs using the small-angle telescope; LA indicates experimental runs using the large-angle telescope.

TABLE VIII. Summary of the mean value of the proton-proton differential scattering cross section for energy of 39.40 Mev.

θ_{lab}	$\theta_{c.m.}$	$d\sigma/d\Omega$ (c.m.) (mb/sterad)	No. of runs	Absolute error (±)	Relative error (±)
4°	8°5′	103.8	6	4.1%	4.0%
5°	10°6′	40.85	3	1.8%	1.7%
6°	12°7′	20.63	3	1.1%	0.9%
7°	14°9′	13.50	4	0.9%	0.6%
8°	16°10′	10.87	4	0.8%	0.5%
8½°	17°11′	10.26	1	0.8%	0.5%
9°	18°11′	10.01	5	0.8%	0.5%
9½°	19°12′	9.98	1	0.8%	0.5%
10°	20°12′	9.79	5	0.8%	0.5%
10½°	21°13′	9.82	2	0.8%	0.5%
11°	22°14′	9.85	4	0.8%	0.5%
11½°	23°14′	9.93	1	0.8%	0.5%
12°	24°15′	9.94	7	0.8%	0.5%
12½°	25°15′	10.07	1	0.8%	0.5%
13½°	27°16′	10.27	3	0.8%	0.5%
15°	30°18′	10.52	4	0.8%	0.5%
18°	36°21′	10.75	2	0.8%	0.5%
20°	40°23′	10.86	3	0.8%	0.5%
22°	44°25′	10.98	2	0.8%	0.5%
25°	50°27′	11.10	4	0.8%	0.5%
28°	56°30′	11.13	2	0.8%	0.5%
30°	60°31′	11.16	3	0.8%	0.5%
32°	64°32′	11.18	1	0.8%	0.5%
35°	70°34′	11.17	4	0.8%	0.5%
38°	76°35′	11.18	1	0.8%	0.5%
40°	80°35′	11.16	3	0.8%	0.5%
45°	90°36′	11.16	3	0.8%	0.5%

[28] Formulas for the relativistic transformation from laboratory to center-of-mass angles and solid angles are given by Chamberlain, Segrè, Tripp, Wiegand, and Ypsilantis, Phys. Rev. **105**, 288 (1957).

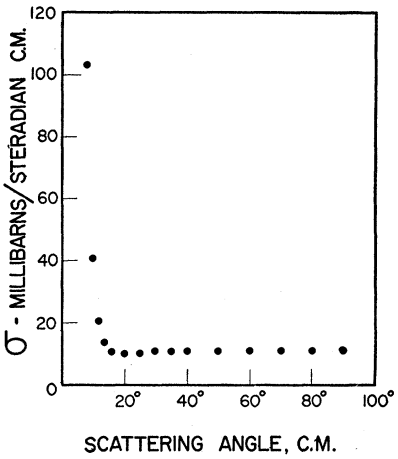

FIG. 11. Gross features of the experimental results.

mental results. Figure 12 shows in more detail the region of the interference minimum and the cross sections extending to 90° (c.m.). The relative experimental error of $\pm\frac{1}{2}\%$ is attached to each point.

IX. DISCUSSION OF RESULTS

A careful phase-shift analysis of these cross sections has been made by Noyes and MacGregor, which appears in an adjoining article.[29] Some of their results may be summarized as follows:

1. The data cannot be fitted by S, P, and D waves alone; a finite amount of F wave is required.

2. A unique set of phase shifts cannot be assigned on the basis of this angular distribution at a single energy, in view of the high-order partial waves involved; good polarization data and energy-dependence data might be able to resolve the ambiguity.

3. The presence of noncentral forces is specifically indicated by the fact that different values are required for the three ^3P phase shifts in any set of phase shifts found to fit the data.

4. A set of phase shifts which fits the data is as follows: $^1S_0$, 40°; $^3P_0$, 16.9°; $^3P_1$, −6.93°; $^3P_2$, 3.04°; $^1D_2$, 2.16°; coupling parameter between $^3P_2$ and $^3F_2$, as defined by Stapp, −2.21°. This is the only solution given which agrees with recent polarization measurements from Harvard at 40 Mev. Noyes and MacGregor indicate that they do not feel that this set of phase shifts is unique.

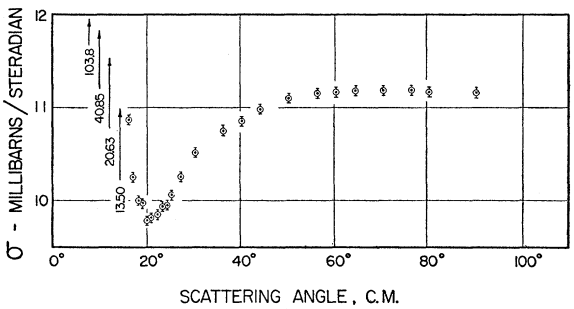

FIG. 12. Partial graph, showing in detail the interference minimum and the cross sections extending to 90° (c.m.). The relative experimental error of $\pm\frac{1}{2}\%$ is attached to each point.

ACKNOWLEDGMENTS

We are indebted to J. H. Williams, A. E. Glassgold, W. B. Cheston, and N. M. Hintz for valuable preliminary discussions of this work. Many helpful suggestions have come to us from H. P. Noyes and M. H. MacGregor in connection with their phase-shift analysis of our preliminary and final data. The mechanical engineering on the scattering chamber was done by E. A. Day and it was constructed under R. B. Thorness' direction. The careful adjustment and operation of the linear accelerator by R. P. Featherstone, D. H. Service, and the operating crew was essential to these results.

[29] H. P. Noyes and M. H. MacGregor, Phys. Rev. 111, 223 (1958), following paper.